Int J Fract (2015) 195:39–52
DOI 10.1007/s10704-015-0047-9

ORIGINAL PAPER

Numerical analysis of crack tip fields in interface fracture of SMA/elastic bi-materials

Arman Afshar · Saeed Hatefi Ardakani · Sepideh Hashemi · Soheil Mohammadi

Received: 1 July 2015 / Accepted: 14 October 2015 / Published online: 29 October 2015

Abstract The problem of an interface crack between a shape memory alloy and an elastic layer is numerically addressed. The shape memory alloy behavior is modeled with a continuum thermodynamics based constitutive model embedded within the finite element method. With the help of the boundary layer approach, and the assumption of small scale transformation zone, the K-dominated region in the tip of the interface crack is loaded under general mixed-mode condition. Both slow and fast loading rates are considered to study the effects of thermo-mechanical coupling on the interface crack tip fields, especially the crack tip energy release rate within a history-dependent J-integral framework, the stress/strain curve during the loading process, and the shape and size of the transformation zone and the heated zone. A special effort is made to investigate how changing the rate of applied loading, the mode-mixity, and the material properties of SMA and elastic layer modify the crack tip fields.

Keywords Bi-material · Interface fracture · Shape memory alloys · Thermo-mechanical coupling

A. Afshar · S. Hatefi Ardakani · S. Hashemi · S. Mohammadi (✉)
High Performance Computing Laboratory, School of Civil Engineering, University of Tehran, Tehran, Iran
e-mail: smoham@ut.ac.ir

1 Introduction

Unique features of shape memory alloy (SMAs) have made these materials popular in different applications, ranging from aerospace structures to piping and medicine industry. SMAs have two different but stable crystallographic phases: austenite and martensite. The reversible thermo-mechanically coupled phase transformation between austenite and martensite is the basis of SMAs' two unique behavior: shape memory effect (SME) and pseudoelasticity (PE). While SME is the capability of recovering large strains and returning to original undeformed shape upon heating, PE refers to the process of forward phase transformation upon loading and reverse phase transformation upon unloading.

The pseudoelasticity phenomenon results in a complex stress distribution near the tip of a crack. Moving from the tip outward, three separate zones of fully martensite, partially martensite and austenite are expected. The outer austenite zone exists far from the crack where the existing stresses are not sufficient enough to initiate the phase transformation ($\xi = 0$). Moving towards the tip of crack, initiation of material transformation results in a partially transformed martensitic zone wherein a mixture of austenite and martensite phases exists ($0 < \xi < 1$). In regions near the crack tip, stress levels are high enough to form the inner fully transformed martensitic zone ($\xi = 1$). The importance of these zones lies beyond their impact on fracture parameters of SMAs.

There are several analytical works on fracture of SMAs. Birman (1998) presented an analytical model to estimate the size of plastic zone in front of the crack tip and subsequently investigated the effect of the phase transformation on the stress intensity factor. Yi and Gao (2000) used the Eshelby inclusion method to analytically demonstrate that the martensite transformation decreases the crack tip stress intensity factor and enhances the fracture toughness of shape memory alloys under mode I loading. An analytical model based on Irwin's correction of linear elastic fracture mechanics was provided by Maletta and Furgiuele (2010) to define the extent of phase transformation in the vicinity of crack tip and the corresponding stress distribution in both transformed and untransformed regions. Baxevanis and Lagoudas (2012) obtained closed form solutions for mode I fracture parameters of a SMA plate utilizing the Dugdale-Barenblatt and derived a relationship between the J-integral and the crack opening displacement.

Among the vast literature that addresses different features of SMAs, there exist only few experimental studies focusing on the fracture of these alloys. Gollerthan et al. (2009) used infrared thermography to examine forward and reverse martensitic transformations in front of a crack tip of SMA compact tension specimens upon loading and unloading, respectively. Robertson et al. (2007) reported three-dimensional strains and phases in front of a propagating fatigue crack in SMAs by combining the synchrotron X-ray microdiffraction with fracture mechanics approaches. Furthermore, Maletta et al. (2013) studied the effect of temperature on stress intensity factor and stress distribution at crack tip vicinity of a shape memory alloy specimen and verified the results numerically. It was reported that increasing the testing temperature could lead in a slight increase in the critical stress intensity factor. Maletta et al. (2014) employed Infrared thermography and digital image correlation techniques to investigate the cyclic temperature and displacement evolutions in the crack tip vicinity in SMAs subjected to fatigue mechanical loads.

In addition to aforementioned studies, several works are devoted to numerical investigation of stress-induced martensite phase transformation ahead of a crack tip. Stam and Van der Giessen (1995), by employing a finite element analysis, investigated how the size and shape of transformation zone and transformation toughening during crack growth were affected by reversible phase transformation. In another work, Wang et al. (2005) implemented Aurichio's model for pseudoelasticity into the ABAQUS code to study the stress-induced martensitic transformation in front of the crack in compact tension specimens. The results revealed that the phase transformation zone in front of the crack tip was parallel with the plastic zone in a material undergoing plastic deformation. Transformation toughening of a slowly propagating mode-I crack was numerically investigated by Freed and Banks-Sills (2007) utilizing a cohesive zone model. Moreover, Wang et al. (2010) reported the changes of martensitic transformation, stress-strain, and failure behavior in front of crack tips in SMAs due to triaxial stress state in plane strain condition. The results demonstrated that in such conditions crack propagation occurred unstably.

Considering the increasing demands of multi-functional needs, SMAs are being used as layers in laminated composites or as fibers in fiber reinforced composites in numerous applications. Many studies have been devoted to the design concepts, constitutive modeling, behavior and micromechanical properties, and self-healing of these composites. For instance, Wei et al. (1997) discussed the design concepts and fabrication of SMA composites. Lagoudas et al. (1997) implemented the layerwise laminate theory of Reddy in a finite element framework for thermo-mechanical analysis of a laminated composite bonded with SMA strips. Furthermore, Shimamoto et al. (2004) conducted a test employing photoelastic method to evaluate the impact of SMAs on enhancement of mechanical strength of NiTi fiber-reinforced epoxy composites and to present an analytical approach based on Eshelby model. Hu et al. (2005) utilized a shear lag model and variational principle to present a failure criterion for an interface crack in SMA fiber reinforce structures with damage. With the assumption of constant temperature, Freed et al. (2008) used the cohesive zone model to study the slowly propagating crack along the interface of a SMA and a linear elastic medium and the consequent transformation toughening. Neuser et al. (2012) investigated the improvement of solvent-based self-healing material with the aim of shape memory alloys by means of reducing the crack face separation and providing internal healing.

To include the effects of thermomechanical coupling, which make the applied loading rate important in simulations, Hatefi Ardakani et al. (2015a) investigated

the impacts of thermo-mechanical coupling effects and loading rates on crack tip fields in homogeneous SMAs. The current study is an extension of Hatefi Ardakani et al. (2015a), with the main objective of investigating fracture parameters of an interface crack. To this end, the problem of an interface crack between a SMA and a linear elastic layer under general mixed-mode fracture is studied by assuming the plane strain condition and a small scale transformation zone.

This paper consists of the following sections. In Sects. 2 and 3, after defining the geometry and boundary conditions of the problem, a brief discussion of constitutive equation and the implementation method is presented. Section 4 presents numerical results of thermo-mechanically coupled fracture analysis of interface crack between SMA and an isotropic elastic medium in the plane strain condition. Finally, a concise conclusion is presented in the last section.

2 Theory and problem statement

Consider the schematic configuration of a bimaterial interface crack as shown in Fig. 1. The crack is located along the interface of two planes, with the upper-half plane being composed of SMA and a linear elastic lower-half plane, denoted with subscripts 1 and 2, respectively. Taking into account the small scale transformation zone, displacements of the K-dominant zone are imposed as the boundary condition. The displacement fields around the crack tip in the upper-half plane are given in Eq. (1). The reader should note that for lower-half plane $\varepsilon\pi$ should be replaced with $-\varepsilon\pi$ (Suo 1989).

$$u_j = \frac{1}{2\mu_1}\sqrt{\frac{r}{2\pi}}\left\{\mathrm{Re}[Kr^{i\varepsilon}]\tilde{u}_j^{\mathrm{I}}(\theta,\varepsilon,\nu_1) + \mathrm{Im}\left[Kr^{i\varepsilon}\right]\tilde{u}_j^{\mathrm{II}}(\theta,\varepsilon,\nu_1)\right\} \quad (j=1,2) \tag{1a}$$

$$\tilde{u}_1^{\mathrm{I}} = A\left[-e^{2\varepsilon(\pi-\theta)}\left(\cos\frac{\theta}{2}+2\varepsilon\sin\frac{\theta}{2}\right) + \kappa_1\left(\cos\frac{\theta}{2}-2\varepsilon\sin\frac{\theta}{2}\right)+\left(1+4\varepsilon^2\right)\sin\frac{\theta}{2}\sin\theta\right] \tag{1b}$$

$$\tilde{u}_1^{\mathrm{II}} = A\left[e^{2\varepsilon(\pi-\theta)}\left(\sin\frac{\theta}{2}-2\varepsilon\cos\frac{\theta}{2}\right) + \kappa_1\left(\sin\frac{\theta}{2}+2\varepsilon\cos\frac{\theta}{2}\right)+\left(1+4\varepsilon^2\right)\cos\frac{\theta}{2}\sin\theta\right] \tag{1c}$$

$$\tilde{u}_2^{\mathrm{I}} = A\left[e^{2\varepsilon(\pi-\theta)}\left(\sin\frac{\theta}{2}-2\varepsilon\cos\frac{\theta}{2}\right) + \kappa_1\left(\sin\frac{\theta}{2}+2\varepsilon\cos\frac{\theta}{2}\right)-\left(1+4\varepsilon^2\right)\cos\frac{\theta}{2}\sin\theta\right] \tag{1d}$$

$$\tilde{u}_2^{\mathrm{II}} = A\left[e^{2\varepsilon(\pi-\theta)}\left(\cos\frac{\theta}{2}+2\varepsilon\sin\frac{\theta}{2}\right) - \kappa_1\left(\cos\frac{\theta}{2}-2\varepsilon\sin\frac{\theta}{2}\right)+\left(1+4\varepsilon^2\right)\sin\frac{\theta}{2}\sin\theta\right] \tag{1e}$$

where (r,θ) are polar coordinates with the origin at the right crack tip. Re[.] and Im[.] denote the real and imaginary parts of complex numbers, respectively. K

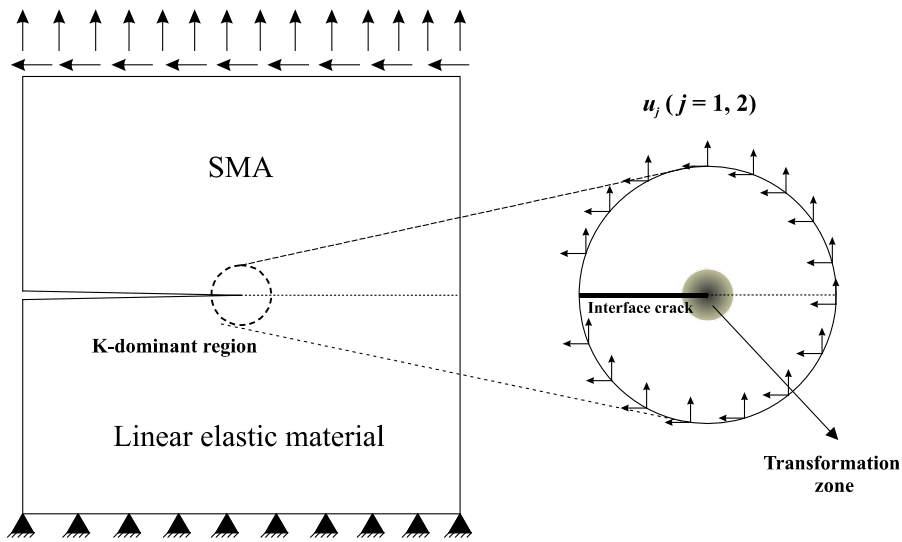

Fig. 1 Configuration of bimaterial interface crack between SMA and linear elastic media

is the complex stress intensity factor, defined as

$$K = K_1 + iK_2 \tag{2}$$

with A

$$A = \frac{e^{-\varepsilon(\pi-\theta)}}{(1+4\varepsilon^2)\cosh(\pi\varepsilon)} \tag{3}$$

The oscillatory parameter ε is a bimaterial constant

$$\varepsilon = \frac{1}{2\pi}\log\left(\frac{1-\beta}{1+\beta}\right) \tag{4}$$

which indicates the mismatch in material properties. In contrast to classical fracture mechanics, oscillatory parameter is no longer constant due to the martensitic region near the crack tip. In Eq. (4), β is the second Dundurs parameter:

$$\beta = \frac{\mu_1(\kappa_2-1)-\mu_2(\kappa_1-1)}{\mu_1(\kappa_2+1)+\mu_2(\kappa_1+1)} \tag{5}$$

$$\kappa_i = 3-4\nu_i \tag{6}$$

where μ_i, ν_i, and κ_i are shear modulus, the Poisson's ratio and the Kolosov constant of material i, respectively, with $i = 1, 2$ for upper and lower half planes.

The phase angle Ψ is a measure of the relation between components of shear and normal stresses along the interface at an arbitrary reference length of $\hat{l}$ at the front of crack, defined as

$$\Psi = \tan^{-1}\left(\frac{\mathrm{Im}\left[K\hat{l}^{i\varepsilon}\right]}{\mathrm{Re}\left[K\hat{l}^{i\varepsilon}\right]}\right) \tag{7}$$

Of utmost importance in fracture study of interface crack is the energy release rate, G, which can be calculated from the J-integral

$$G = J = \int_\Gamma \left(\mathbf{n}\cdot\boldsymbol{\sigma}\cdot\frac{\partial\mathbf{u}}{\partial x_1} - Wn_1\right)\mathrm{d}s \tag{8}$$

or alternatively,

$$\begin{aligned} J = \int_\mathrm{A} \Bigg(&\frac{\partial q}{\partial\mathbf{x}}\cdot\boldsymbol{\sigma}\cdot\frac{\partial\mathbf{u}}{\partial x_1} \\ &-W\frac{\partial q}{\partial x_1} + \alpha\cdot\mathrm{tr}(\boldsymbol{\sigma})\cdot\frac{\partial T}{\partial x_1}\cdot q\Bigg)\,\mathrm{d}A \\ &-\int_\mathrm{A}\mathbf{f}\cdot\frac{\partial\mathbf{u}}{\partial x_1}\cdot q\,\mathrm{d}A - \int_{C^+ + C^-}\mathbf{t}\cdot\frac{\partial\mathbf{u}}{\partial x_1}\cdot q\,\mathrm{d}C \end{aligned} \tag{9}$$

where q is an arbitrary function ranging from $q = 1$ at the inner region A to $q = 0$ at the outer boundary. $\mathbf{f}$ and $\mathbf{t}$ are body force per unit volume and traction on the crack surface, respectively, and in this study are equivalent to zero.

While for non-dissipative materials (such as nonlinear elastic materials), the value of J-integral is independent of the chosen contour of integration, for the dissipative materials (such as elastic-plastic materials and SMAs) the J-integral depends on the chosen contours. This inconsistency is due to plastic strain in the crack tip of elastic-plastic materials, as discussed in Carka and Landis (2011), Carka et al. (2012) and the martensitic transformed zone near the crack tip in SMAs, as discussed in Baxevanis et al. (2012). At far-enough distances, however, the J-integral retains its path-independent characteristic.

The reference J-integral, calculated in the austenite region, and associated with the applied boundary condition is defined as

$$G_{applied} = \frac{1}{E^*}\left(\frac{|K|^2}{\cosh^2(\pi\varepsilon)}\right) \tag{10}$$

where

$$|K|^2 = K\overline{K} = K_\mathrm{I}^2 + K_\mathrm{II}^2 \tag{11a}$$

$$\frac{2}{E^*} = \frac{1}{\overline{E_1}} + \frac{1}{\overline{E_2}} \tag{11b}$$

$$\overline{E_i} = \frac{E_i}{1-\upsilon_i^2} \tag{11c}$$

3 The constitutive model of SMA

This section provides a brief discussion on thermo-mechanical behavior of polycrystalline SMAs utilizing a fully coupled constitutive equation. The constitutive equation of SMAs has been studied in several works, mostly based on either the Helmholtz free energy (Brinson 1993; Leclercq and Lexcellent 1996; Juhasz et al. 2002; Helm and Haupt 2003; Paiva et al. 2005; Reese and Christ 2008) or the Gibbs free energy (Sun and Hwang 1983a, b; Boyd and Lagoudas 1996; Qidwai and Lagoudas 2000; Lagoudas and Entchev 2004; Popov and Lagoudas 2007; Ahmadian et al. 2015). In order to capture the thermo-mechanical response of SMAs, this study employs the Gibbs based constitutive equation of Boyd and Lagoudas (1996).

Considering the infinitesimal strain theory, the additive decomposition allows the total strain to be decomposed into thermo-elastic $\varepsilon^{\mathrm{thermo-elastic}}$ and transformation ε^{t} parts,

$$\varepsilon^{\text{total}} = \varepsilon^{\text{thermo-elastic}} + \varepsilon^{\text{t}} \tag{12}$$

As discussed in Baxevanis et al. (2012), the plastic zone is highly suppressed due to the phase transformation of SMAs and only a very small section of fully transformed martensitic region deforms plastically. Consequently, the plastic strain is disregarded in the discretized strain form of Eq. (12).

To formulate the constitutive equation, the stress tensor $\boldsymbol{\sigma}$, temperature T, and transformation strain ε^t are chosen as the external state variables and the martensitic volume fraction ξ is considered as the internal state variable. The specific Gibbs free energy can be written as (Boyd and Lagoudas 1996; Qidwai and Lagoudas 2000)

$$\begin{aligned} G_s(\boldsymbol{\sigma}, T, \varepsilon^{\text{t}}, \xi) &= -\frac{1}{2\rho}\boldsymbol{\sigma} : \mathbf{S} : \boldsymbol{\sigma} - \frac{1}{\rho}\boldsymbol{\sigma} : \left(\boldsymbol{\alpha}(T - T_0) + \varepsilon^{\text{t}}\right) \\ &\quad + c\left((T - T_0) - T\ln\left(\frac{T}{T_0}\right)\right) - s_0 T \\ &\quad + u_0 + \frac{1}{\rho}\eta(\xi) \end{aligned} \tag{13}$$

where ρ, c, s_0 and u_0 are material density, the effective specific heat, the effective specific entropy and the effective specific internal energy, respectively. $\boldsymbol{\alpha}$ and $\mathbf{S}$ are the effective thermal expansion and compliance tensors. $\eta(\xi)$ is the polynomial transformation hardening function (see Boyd and Lagoudas 1996).

The effective material parameters during phase transformation are defined using a linear relation proposed by Boyd and Lagoudas (1996).

Note that $\xi = 0$ and $\xi = 1$ represent pure austenite and martensite phases, respectively.

The total strain can be obtained from the specific Gibbs free energy,

$$\boldsymbol{\varepsilon} = -\rho\frac{\partial G_{\text{s}}}{\partial \boldsymbol{\sigma}} = \mathbf{C} : \boldsymbol{\sigma} + \boldsymbol{\alpha}(T - T_0) + \boldsymbol{\varepsilon}^{\text{t}} \tag{14}$$

The transformation tensor relates the transformation strain to the martensitic volume fraction

$$\dot{\boldsymbol{\varepsilon}}^{\text{t}} = \boldsymbol{\Lambda}\dot{\xi} \tag{15}$$

The transformation tensor during the forward transformation ($\dot{\xi} > 0$) is presented as

$$\boldsymbol{\Lambda} = \frac{3}{2}H\frac{\boldsymbol{\sigma}_{\text{dev}}}{\sigma_{\text{eff}}} \tag{16}$$

where H, $\boldsymbol{\sigma}_{\text{dev}}$ and σ_{eff} are the maximum transformation strain, the deviatoric stress tensor and the von Mises stress, respectively.

Employing the Clausius-Planck inequality, the thermodynamic force Π conjugated to ξ for the specific Gibbs free energy can be defined as,

$$\begin{aligned} \Pi(\boldsymbol{\sigma}, T, \xi) &= \boldsymbol{\sigma} : \boldsymbol{\Lambda} + \frac{1}{2}\boldsymbol{\sigma} : \Delta\mathbf{S} : \boldsymbol{\sigma} + \boldsymbol{\sigma} : \Delta\boldsymbol{\alpha}(T - T_0) \\ &\quad - \rho\Delta c\left((T - T_0) - T\ln\left(\frac{T}{T_0}\right)\right) \\ &\quad + \rho\Delta s_0 T - \rho\Delta u_0 + \frac{\partial\eta}{\partial\xi} \end{aligned} \tag{17}$$

The bottom line assumption of phase transformation is that the phase transformation initiates only if the thermodynamic force Π reaches its limit

$$\Phi = \Pi - X = 0 \tag{18}$$

where Φ is the transformation surface. X is the material parameter given as

$$X = \frac{1}{4}\rho\Delta s_0\left(T_{\text{s}}^{\text{M}} + T_{\text{f}}^{\text{M}} - T_{\text{s}}^{\text{A}} - T_{\text{f}}^{\text{A}}\right) \tag{19}$$

where T_{s}^{M}, T_{f}^{M},T_{s}^{A} and T_{f}^{A} are the martensite start and finish temperatures, and the austenite start and finish temperatures, respectively.

The mechanical balance equation of the K-dominant domain and its associated boundary conditions are

$$\nabla \cdot \boldsymbol{\sigma} + \mathbf{f}_{\text{b}} = 0 \tag{20a}$$

$$\boldsymbol{\sigma} \cdot \mathbf{n} = \mathbf{t} \text{ on } \Gamma_{\text{t}} \tag{20b}$$

$$\mathbf{u} = \bar{\mathbf{u}} \text{ on } \Gamma_{\text{u}} \tag{20c}$$

where $\bar{\mathbf{u}}$ is obtained from Eq. (1a).

To account for temperature coupling effects during the forward phase transformation, the heat equation should be solved. The coupled heat equation and its boundary conditions are

$$T\boldsymbol{\alpha} : \dot{\boldsymbol{\sigma}} + \rho c\dot{T} + (-\Pi + \rho\Delta s_0 T)\dot{\xi} = \nabla \cdot \mathbf{q} \tag{21a}$$

$$T = T^s \text{ on } S_T \tag{21b}$$

$$k_n\frac{\partial T}{\partial \mathbf{n}} = q^s = h(T_{ext}^S - T^S) \text{ on } S_q \tag{21c}$$

where $\mathbf{q}$, T^s, k_n, $\mathbf{n}$, and q^s are the heat flow, the prescribed temperature on surface S_T, the thermal conductivity, the normal unit vector and the prescribed heat flux on surface S_q, respectively.

To numerically solve the discretized form of balance and heat equations the Newton-Raphson method is utilized. A more detailed discussion of the thermo-mechanical coupling algorithm is provided in Ahmadian et al. (2015). Considering the return mapping algorithm, the interested reader should refer to the algorithm fully discussed in Qidwai and Lagoudas (2000).

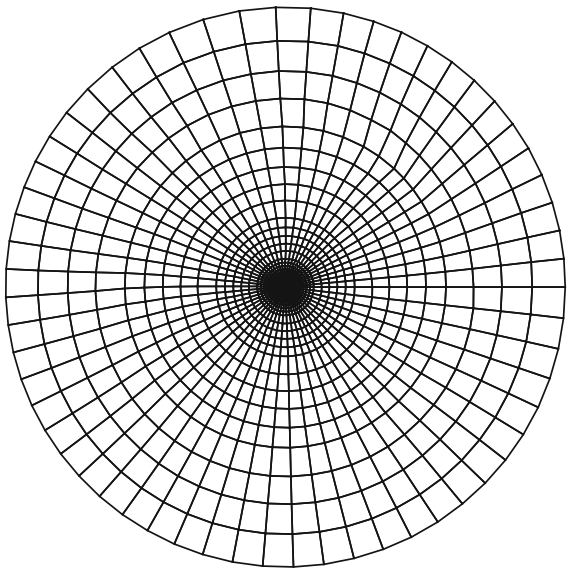

Fig. 2 The finite element mesh of 4320 quadrilateral elements

Table 1 SMA material properties

Material parameters	Values	Material parameters	Values
E_A (GPa)	47	T_s^A (°C)	26
E_M (GPa)	24	T_f^A (°C)	12
υ_A	0.33	C_A (MPa °C^{-1})	8.4
υ_M	0.33	C_M (MPa °C^{-1})	6.7
H	0.05	k_n (W m^{-1} K^{-1})	18.3
T_0 (°C)	35	ρ (kg m^{-3})	6500
T_f^M (°C)	−29	c (J kg^{-1} K^{-1})	837
T_s^M (°C)	3		

4 Results and discussions

In this section, fracture parameters of an interface crack under mixed-mode condition are numerically investigated employing a fully coupled thermo-mechanical constitutive model. Invoking the assumption of small scale transformation zone, the analysis is performed on a 4320 element mesh (as shown in Fig. 2) under the plane strain condition. The material properties of SMA, adopted from Baxevanis et al. (2014), are presented in Table 1. The material properties of the elastic layer are: $E = 30$ GPa, $\nu = 0.25$. Moreover, the perimeter of the circle shown in Fig. 1 is considered as the thermal boundary condition with the prescribed values of ambient temperature.

In order to study the impact of mode-mixity, ranging from $\Psi = 0°$ to $\Psi = 90°$, on changes of energy release rate, the values of K_I and K_{II} are chosen in a way that results in the same value of $R_\xi = 0.03$ in all mode-mixities. Then, the corresponding applied energy release rate is calculated from Eq. (10). Note that in this contribution, the time ratio of applied energy release rate ($\dot{G}_{applied} = G_{applied}/\text{total time}$) is considered as the applied loading rate, as presented in Table 2 for different phase angles (Ψ).

The calculated energy release rates are presented in Fig. 3. It is observed that the curves corresponding to $\Psi = 0°$ and $\Psi = 90°$ are the lower and upper boundaries of other mixed-mode loading curves, respectively. The curves of mode-mixities of $\Psi = 0°, 15°$, and $30°$ have a minimum bellow the line $G/G_{applied} = 1$, while all other mode-mixities are entirely located above the aforementioned line. It is worth mentioning that the calculated values of the energy release rate become the far field $\dot{G}_{\text{applied}}$, as expected.

The phase transformation contours are depicted in Fig. 4. It is clearly observed that the occurred transformation in the upper-half SMA plane follows the far field mode-mixities.

Table 2 Applied loading rates

$\dot{G}_{\text{applied}}\left(\frac{\text{N}}{\text{mm s}}\right)$	$\Psi = 0°$	$\Psi = 15°$	$\Psi = 30°$	$\Psi = 45°$	$\Psi = 60°$	$\Psi = 75°$	$\Psi = 90°$
Loading rate I	0.481	0.370	0.227	0.148	0.145	0.156	0.124
Loading rate II	4.81	3.70	2.27	1.48	1.45	1.82	2.47
Loading rate III	48.1	37.0	22.7	14.8	14.2	18.2	24.7

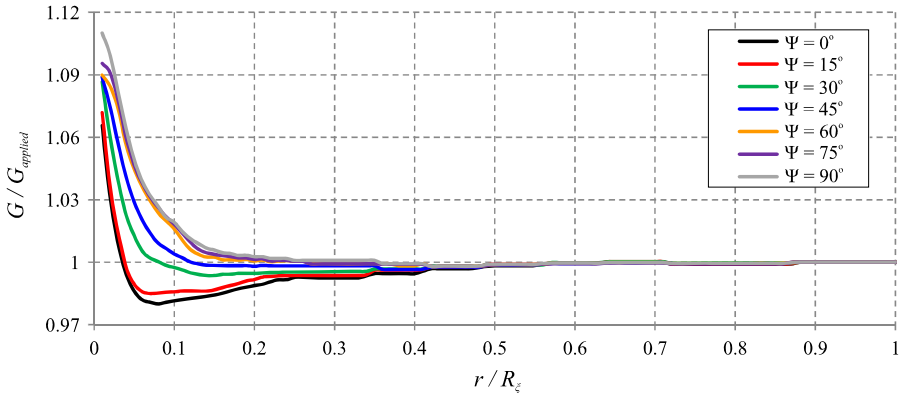

Fig. 3 Calculated energy release rates for different values of mode-mixities

It should be noted that as a result of generated latent heat during the forward transformation, ignoring the thermo-mechanical coupling effects on fracture analysis of crack tip is neither feasible nor plausible. The temperature distributions around the interface crack tip for all values of the phase angles at the loading rate III are depicted in Fig. 5. It is apparent that the shape of heated zone rotates in similar manner to the mode-mixities. It is also observed that because of its conductive nature, temperature distributes well into the elastic medium.

The magnitude and time span of applied loading are two effective parameters that determine the value of generated latent heat. More latent heat is released for higher applied loading rates during the forward transformation, which in turn significantly affects the crack tip fields. To investigate these effects, the following simulation is presented for an uncoupled case along with three different loading rates.

Variation of the energy release rate versus the distance from crack tip is plotted in Fig. 6 for the cases of $\Psi = 0°, 90°$, demonstrating that the available energy for crack growth decreases as a result of the released heat. Figure 6 shows that there exists a critical distance from the crack tip wherein the latent heat effects remain important. While this critical distance for $\Psi = 0°$ is $r/R_{\xi} = 0.09$, it extends to $r/R_{\xi} = 0.2$ for $\Psi = 90°$. Thereby, It can be concluded that at $\Psi = 0°$, the coupling effect of latent heat decreases in a shorter span in comparison with the case of $\Psi = 90°$. In another words, the critical distance becomes larger with the mode-mixity shifting from $\Psi = 0°$ to $\Psi = 90°$.

It is apparent that the coupling effects modify the stress distribution around the crack tip. The von Mises stress-strain response of a point near the crack tip for $\Psi = 0°$ is plotted in Fig. 7. The less the time span of applied loading, the more stress is increased in the partially transformed material. Moreover, Fig. 7 shows that as the rate of applied loading rate decreases the strain in which the phase transformation completes becomes smaller ($\varepsilon_4 < \varepsilon_3 < \varepsilon_2 < \varepsilon_1$). Since material points farther from the crack tip experience smaller strains, the zone of complete phase transformation ($\xi = 1$) becomes larger in slower loading rates. This interesting phenomenon is presented in Fig. 8 in which the martensitic boundary ($\xi = 1$) is depicted for different values of phase angle ($\Psi = 0°, 45°$, and $90°$) at different loading rates. It is observed that by increasing the applied loading rate, the strain corresponding with martensitic transformation completion increases, and consequently, the available time devoted to completion of phase transformation of material points lessens. This matter is equivalent to the fact that less material points reach the completion of martensitic transformation, leading to smaller zone of complete phase transformation.

To investigate the effect of ambient temperature, the energy release rate of crack tip for $\Psi = 0°$ is presented in Fig. 9 for four different ambient temperatures: 30, 35, 40, and 45 °C. As reported by Baxevanis et al. (2012) for a homogeneous SMA, it can be seen that by increasing the ambient temperature, the available energy for crack growth decreases.

In order to study the effect of Young's modulus of the elastic material on the energy release rate of crack tip, simulations are performed in different cases and the results are depicted in Fig. 10. The chosen values of Young's modulus of the elastic lower-plane are

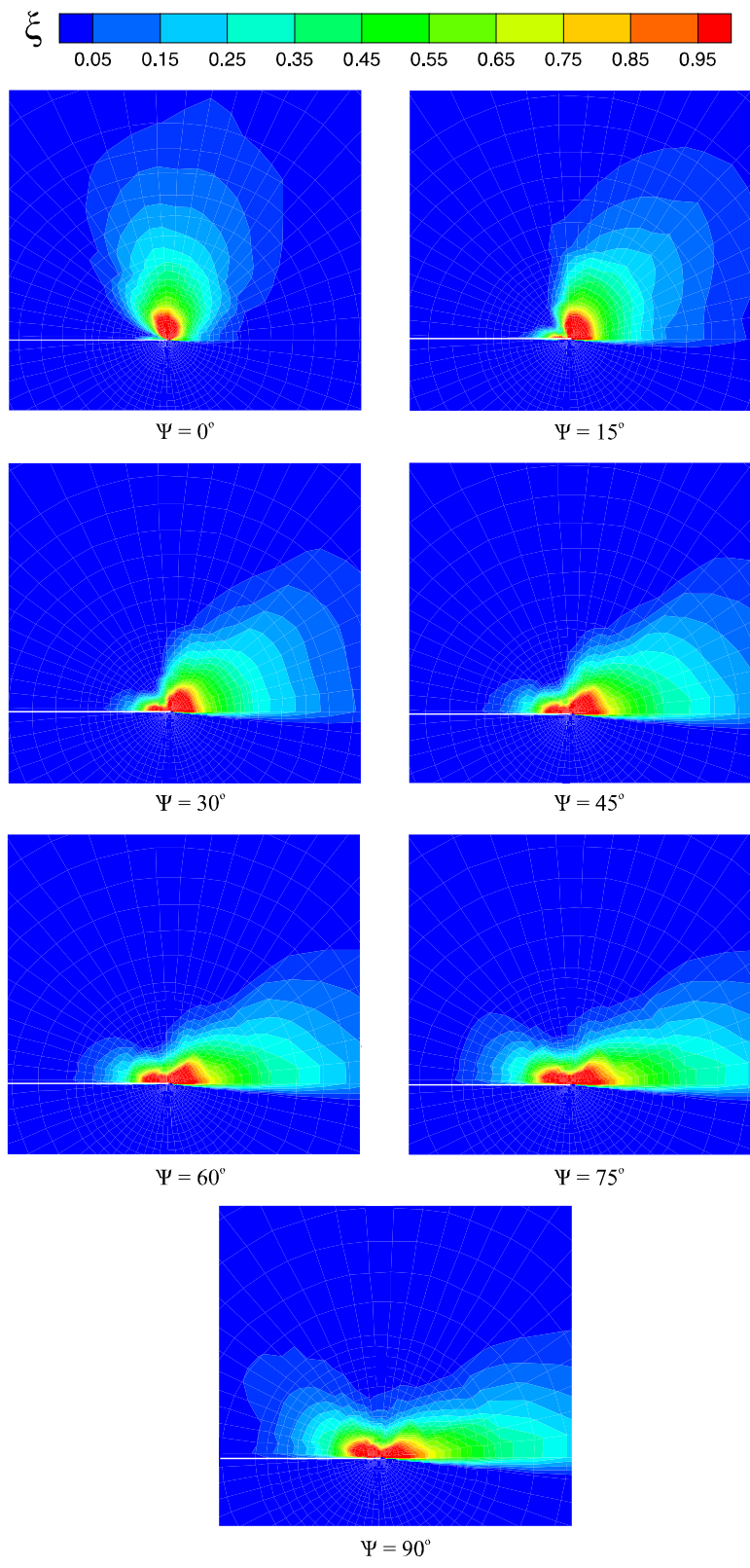

Fig. 4 Phase transformation contours for different phase angels

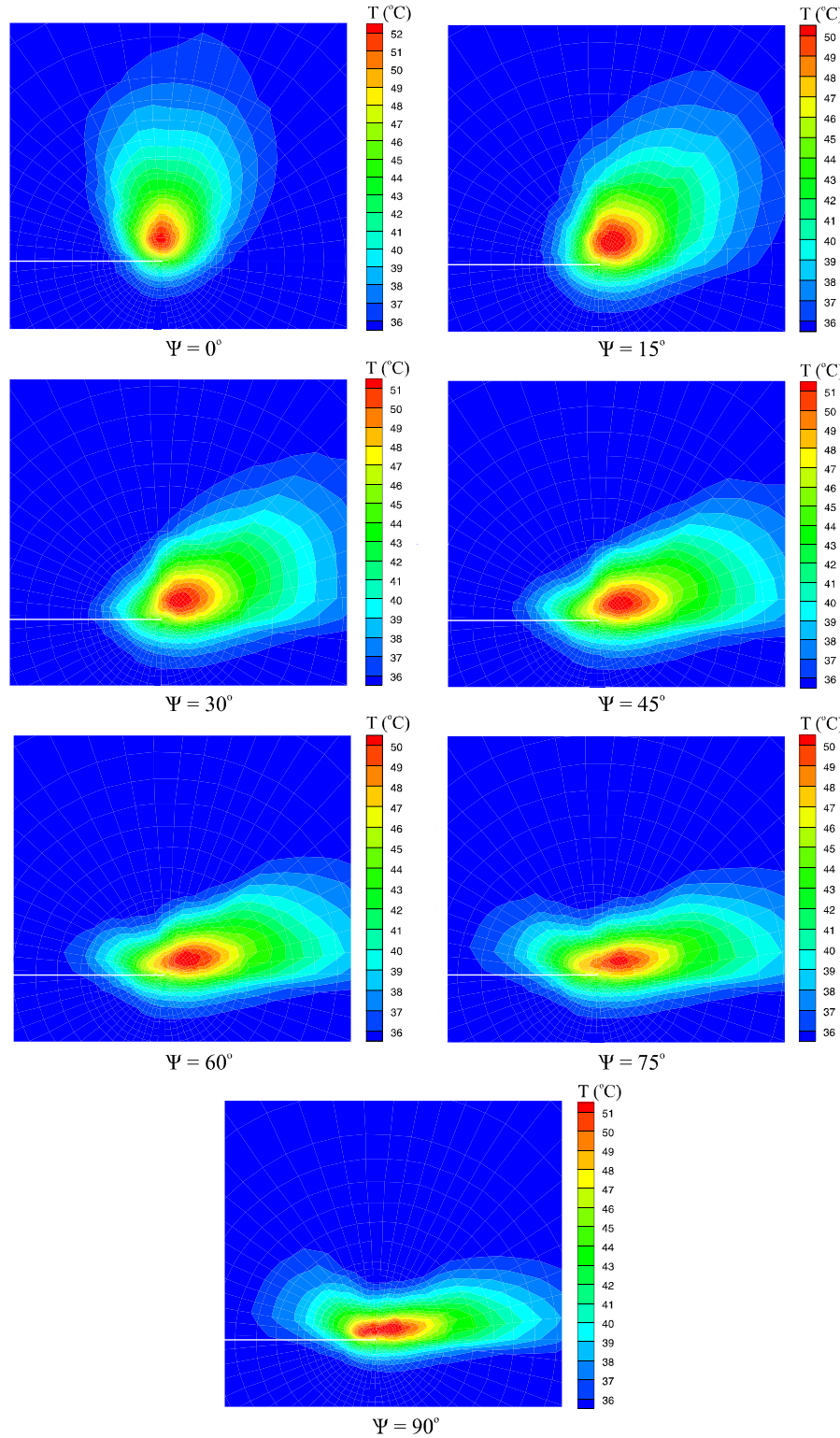

Fig. 5 Temperature distribution for different phase angels

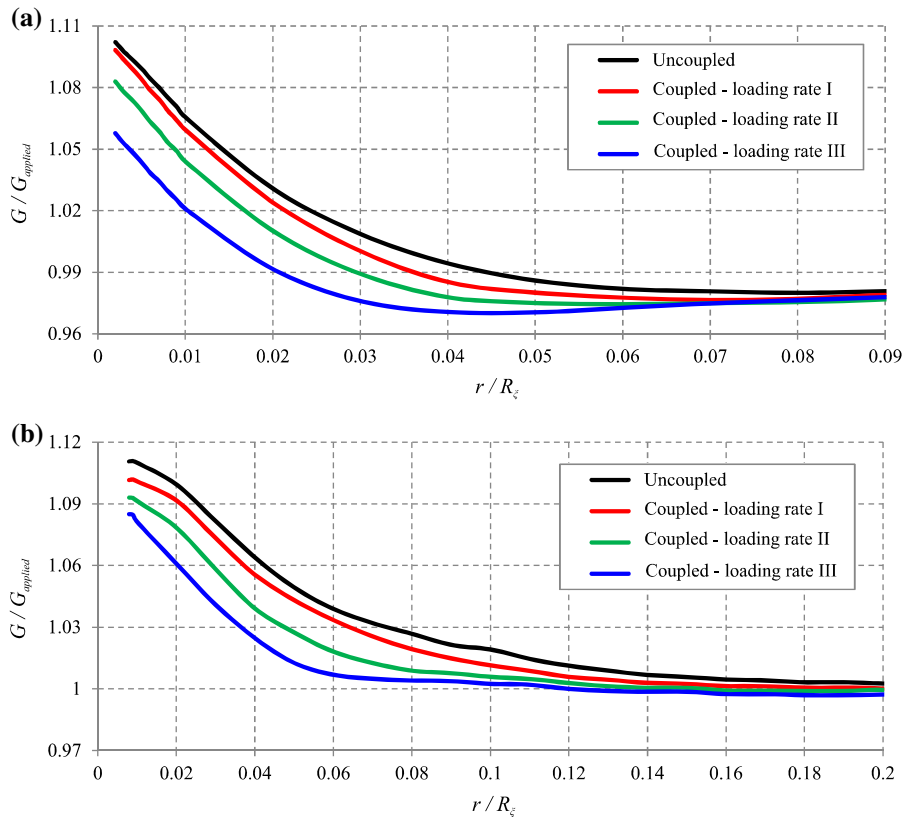

Fig. 6 The impact of applied loading rate on the energy release rate of crack tip **a** $\Psi = 0°$, **b** $\Psi = 90°$

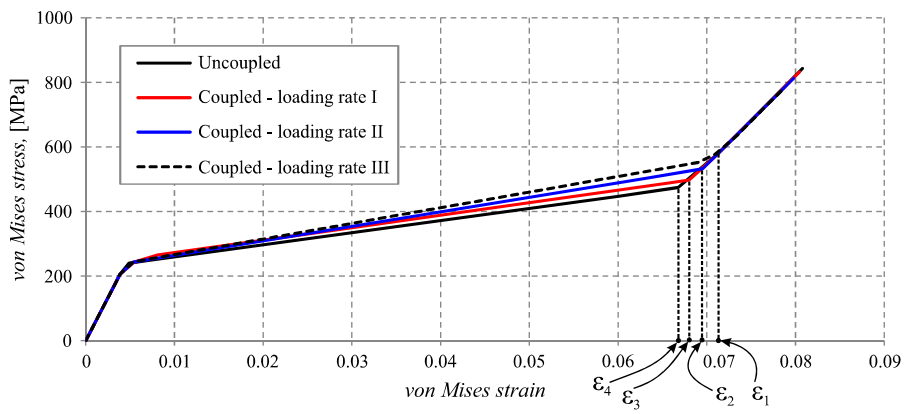

Fig. 7 The impact of applied loading rate on the local von Mises stress-strain curve for a point near the crack tip

$E^{\text{elastic}} = 30, 60, 100,$ and 200 GPa. It is observed that near the crack tip the increase of E^{elastic} results in an increase of the energy release rate. However, the diagrams converge at a distance of $0.05R_\xi$ and the trends slightly reverse afterwards; i.e. reduced energy release rate for higher values of E^{elastic}.

Figure 11 illustrates the influence of maximum transformation strain (H) on size of the phase transformation regions ($\xi = 1$) for the given values of phase angles of $\Psi = 0°, 45°,$ and $90°$. It can be seen that the increase of H leads to smaller boundaries of the transformation zone. This is primarily due to the fact that as H decreases, the phase transformation completes sooner, providing more time for more material points to reach the martensitic ratio of 1 ($\xi = 1$), consequently the transformation zone will experience a growth in its size. Note that similar observations have already been reported for homogeneous SMAs, both analyt-

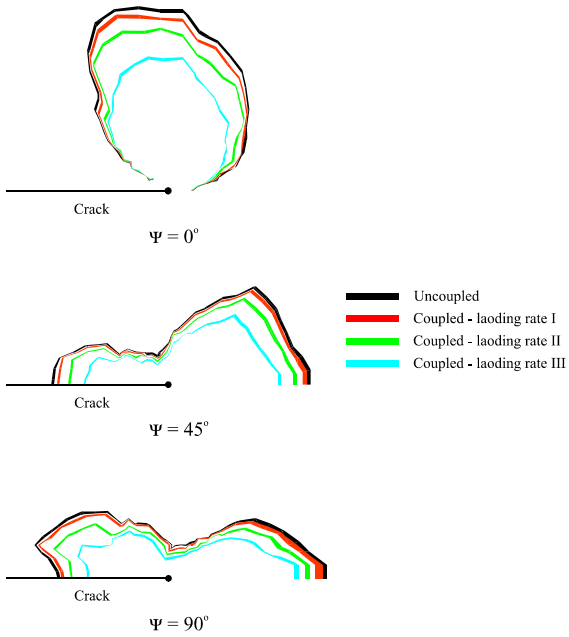

Fig. 8 Effect of applied loading rate on the martensitic boundary for $\Psi = 0°, 45°,$ and $90°$

ically (Maletta and Furgiuele 2010) and numerically (Hatefi Ardakani et al. 2015b).

5 Conclusion

Using finite element analysis and the boundary layer approach, the effects of thermo-mechanical coupling on mixed-mode crack tip fields in an interface crack between a SMA and an elastic layer are addressed. It has been shown that increasing the rate of the applied loading decreases the available energy for crack growth, while increasing the stress during the forward phase transformation. A smaller transformation zone is also observed in higher loading rates. Moreover, a decrease in the crack tip energy release rate is observed by increasing the ambient temperature. A similar result is also observed by decreasing the Young's modulus of the elastic layer. Finally the simulations have demonstrated that an increase in the maximum transformation strain makes the transformation zone smaller.

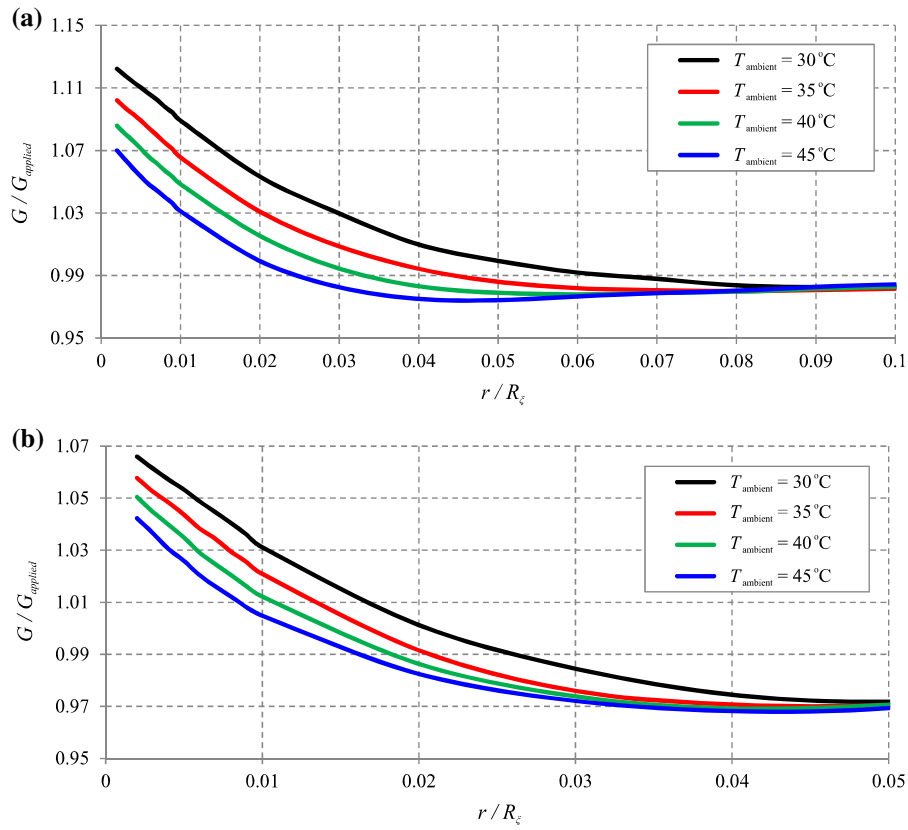

Fig. 9 Influence of ambient temperature on energy release rate of crack tip **a** isothermal condition, **b** loading rate III

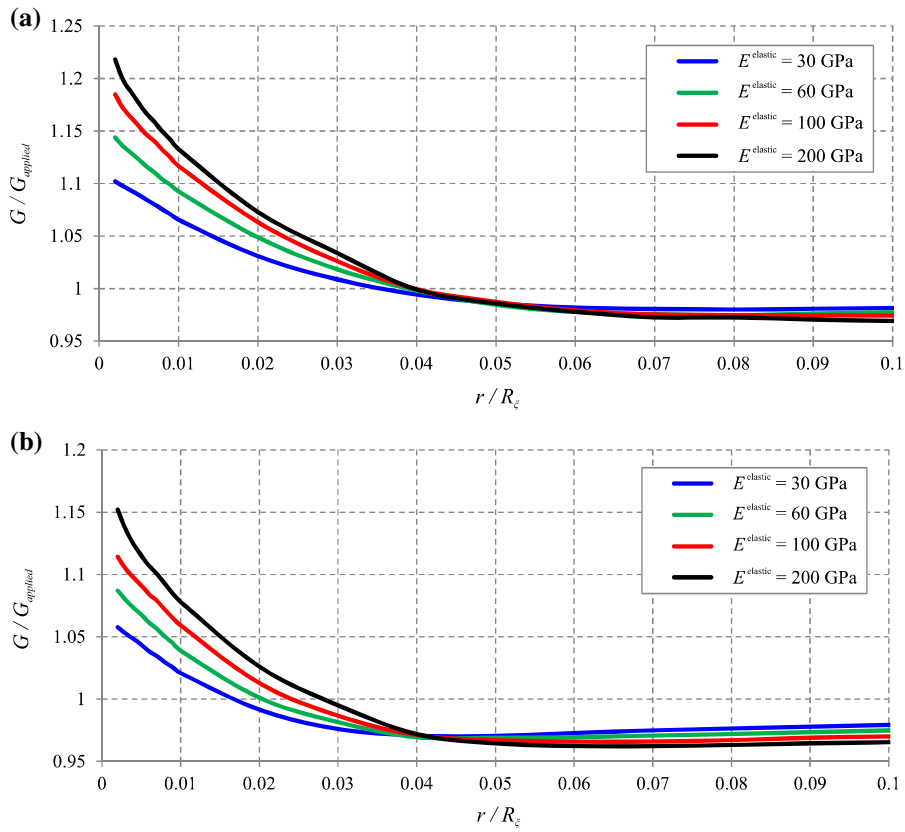

Fig. 10 Effect of the Young's modulus of the elastic lower-half medium on the energy release rate **a** isothermal condition, **b** loading rate III

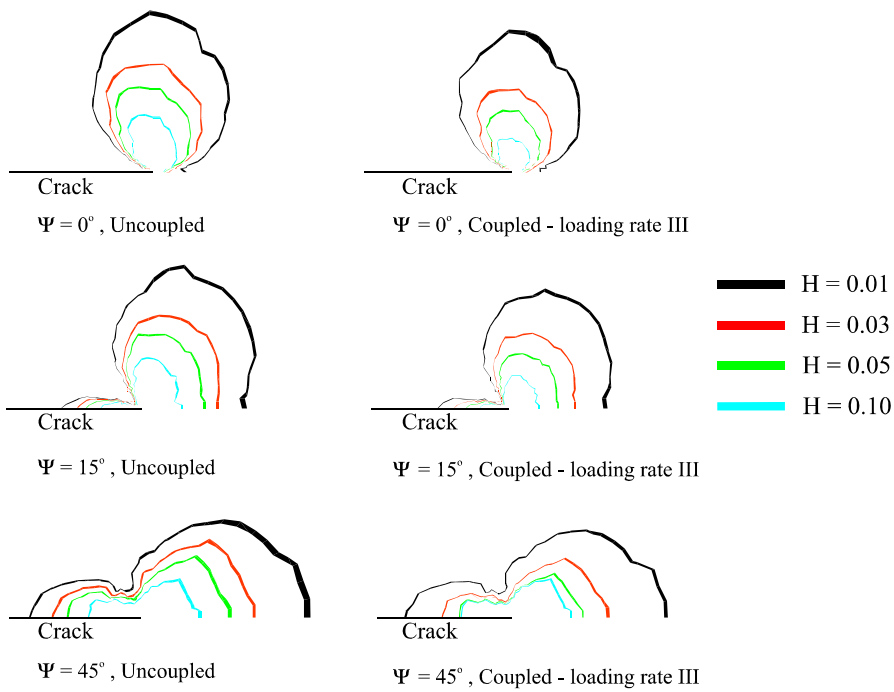

Fig. 11 Effect of maximum transformation strain on the martensitic boundary for $\psi = 0°, 15°,$ and $45°$

Acknowledgments The authors wish to acknowledge the technical support of the High Performance Computing Lab, School of Civil Engineering, University of Tehran. The financial support of Iran National Science Foundation (INSF) is gratefully acknowledged.

References

Ahmadian H, Hatefi Ardakani S, Mohammadi S (2015) Strain-rate sensitivity of unstable localized phase transformation phenomenon in shape memory alloys using a non-local model. Int J Solids Struct 63:167–183

Baxevanis T, Chemisky Y, Lagoudas DC (2012) Finite element analysis of the plane-strain crack-tip mechanical fields in pseudoelastic shape. Mem Alloys Smart Mater Struct 21:094012

Baxevanis T, Lagoudas DC (2012) A mode I fracture analysis of a center-cracked infinite shape memory alloy plate under plane stress. Int J Fract 175:151–166

Baxevanis T, Landis CM, Lagoudas DC (2014) On the fracture toughness of pseudoelastic shape memory alloys. J Appl Mech 81(4):041005

Birman V (1998) On mode I fracture of shape memory alloy plates. Smart Mater Struct 7:433

Boyd JG, Lagoudas DC (1996) A thermodynamical constitutive model for shape memory materials. Part I. The monolithic shape memory alloy. Int J Plast 12:805–842

Brinson LC (1993) One-dimensional constitutive behavior of shape memory alloys: thermomechanical derivation with non-constant material functions and redefined martensite internal variable. J Intell Mater Syst Struct 4:229–242

Carka D, Landis CM (2011) On the path-dependence of the J-integral near a stationary crack in an elastic-plastic material. J Appl Mech 78:011006

Carka D, McMeeking RM, Landis CM (2012) A note on the path-dependence of the J-integral near a stationary crack in an elastic-plastic material with finite deformation. J Appl Mech 79:044502

Freed Y, Banks-Sills L (2007) Crack growth resistance of shape memory alloys by means of a cohesive zone model. J Mech Phys Solids 55:2157–2180

Freed Y, Banks-Sills L, Aboudi J (2008) On the transformation toughening of a crack along an interface between a shape memory alloy and an isotropic medium. J Mech Phys Solids 56:3003–3020

Gollerthan S, Young M, Neuking K, Ramamurty U, Eggeler G (2009) Direct physical evidence for the back-transformation of stress-induced martensite in the vicinity of cracks in pseudoelastic NiTi shape memory alloys. Acta mater 57:5892–5897

Hatefi Ardakani S, Afshar A, Mohammadi S (2015a) Numerical study of thermo-mechanical coupling effects on crack tip fields of mixed-mode fracture in pseudoelastic shape memory alloys (under revision)

Hatefi Ardakani S, Ahmadian H, Mohammadi S (2015b) Thermo-mechanically coupled fracture analysis of shape memory alloys using the extended finite element method. Smart Mater Struct 24:045031

Helm D, Haupt P (2003) Shape memory behavior: modelling within continuum thermomechanics. Int J Solids Struct 40:827–849

Hu Z, Xiong K, Wang X (2005) Study on interface failure of shape memory alloy (SMA) reinforced smart structure with damages. Acta Mech Sin 21:286–293

Juhasz L, Schnack E, Hesebeck O, Andra H (2002) Macroscopic modeling of shape memory alloys under non-proportional themo-mechanical loadings. J Intell Mater Syst Struct 13:825–836

Lagoudas DC, Entchev PB (2004) Modeling of transformation-induced plasticity and its effect on the behavior of porous shape memory alloys. Part I: constitutive model for fully dense SMAs. Mech Mater 36:865–892

Lagoudas DC, Moorthy D, Qidwai MA, Reddy JN (1997) Modeling of the thermomechanical response of active laminates with SMA strips using the layerwise finite element method. J Intell Mater Syst Struct 8:476–488

Leclercq S, Lexcellent C (1996) A general macroscopic description of the thermomechanical behavior of shape memory alloys. J Mech Phys Solids 44:953–980

Maletta C, Bruno L, Corigliano P, Crupi V, Guglielmino E (2014) Crack-tip thermal and mechanical hysteresis in shape memory alloys under fatigue loading. Mater Sci Eng A 616:281–287

Maletta C, Furgiuele F (2010) Analytical modeling of stress-induced martensitic transformation in the crack tip region of nickel-titanium alloys. Acta Mater 58:92–101

Maletta C, Sgambitterra E, Furgiuele F (2013) Crack tip stress distribution and stress intensity factor in shape memory alloys. Fatigue Fract Eng Mater Struct 36:903–912

Neuser S, Michaud V, White SR (2012) Improving solvent-based self-healing materials through shape memory alloys. Polymer 53:370–378

Paiva A, Savi MA, Bragra AMB, Pachec PMCL (2005) A constitutive model for shape memory alloys considering tensile-compressive asymmetry and plasticity. Int J Solids Struct 42:3439–3457

Popov P, Lagoudas DC (2007) 3-D constitutive model for shape memory alloys incorporating pseudoelasticity and detwinning of selfaccommodated martensite. Int J Plast 23:1679–1720

Qidwai MA, Lagoudas DC (2000) On thermomechanics and transformation surfaces of polycrystalline NiTi shape memory alloy material. Int J Plast 16:1309–1343

Reese S, Christ D (2008) Finite deformation pseudo-elasticity of shape memory alloys—constitutive modelling and finite element implementation. Int J Plast 24:455–482

Robertson SW, Metha A, Pelton AR, Ritchie RO (2007) Evolution of crack-tip transformation zones in superelastic Nitinol subjected to in situ fatigue: a fracture mechanics and synchrotron X-ray micro-di raction analysis. Acta Mater 55:6198–6207

Shimamoto A, Ohkawara H, Nogata F (2004) Enhancement of mechanical strength by shape memory effect in TiNi fiber-reinforced composites. Eng Fract Mech 71:737–746

Stam G, Van der Giessen E (1995) Effect of reversible phase transformations on crack growth. Mech Mater 21:51–71

Sun QP, Hwang KC (1983a) Micromechanics modelling for the constitutive behavior of polycrystalline shape mem-

ory alloys-II. Study of individual phenomena. J Mech Phys Solids 41:19–33

Sun QP, Hwang KC (1983b) Micromechanics modelling for the constitutive behavior of polycrystalline shape memory alloys-I. Derivation of general relations. J Mech Phys Solids 41:1–17

Suo Z (1989) Mechanics of interface fracture. PhD Thesis, Harvard University, Cambridge, p 103

Wang G, Xuan F, Tu S, Wang Z (2010) Effects of triaxial stress on martensite transformation, stress-strain and failure behavior in front of crack tips in shape memory alloy NiTi. Mater Sci Eng A 527:1529–1536

Wang X, Wang Y, Baruj A, Eggeler G, Yue Z (2005) On the formation of martensite in front of cracks in pseudoelastic shape memory alloys. Mater Sci Eng A 394:393–398

Wei ZG, Tang CY, Lee W (1997) Design and fabrication of intelligent composites based on shape memory alloys. J Mater Process Technol 69:68–74

Yi S, Gao S (2000) Fracture toughening mechanism of shape memory alloys due to martensite transformation. Int J Solids Struct 37:5315–5327